ChemComm

Accepted Manuscript

This article can be cited before page numbers have been issued, to do this please use: T. J. Penfold, F. Dias and A. P. Monkman, *Chem. Commun.*, 2018, DOI: 10.1039/C7CC09612G.

This is an Accepted Manuscript, which has been through the Royal Society of Chemistry peer review process and has been accepted for publication.

Accepted Manuscripts are published online shortly after acceptance, before technical editing, formatting and proof reading. Using this free service, authors can make their results available to the community, in citable form, before we publish the edited article. We will replace this Accepted Manuscript with the edited and formatted Advance Article as soon as it is available.

You can find more information about Accepted Manuscripts in the author guidelines.

Please note that technical editing may introduce minor changes to the text and/or graphics, which may alter content. The journal's standard Terms & Conditions and the ethical guidelines, outlined in our author and reviewer resource centre, still apply. In no event shall the Royal Society of Chemistry be held responsible for any errors or omissions in this Accepted Manuscript or any consequences arising from the use of any information it contains.

ROYAL SOCIETY OF CHEMISTRY

rsc.li/chemcomm

View Article Online
DOI: 10.1039/C7CC09612G
ROYAL SOCIETY OF CHEMISTRY

Journal Name

ARTICLE TYPE

Cite this: DOI: 10.1039/xxxxxxxxxx

The Theory of Thermally Activated Delayed Fluorescence for Organic Light Emitting Diodes.

T.J. Penfold*[a], F.B Dias[b] and A.P. Monkman[b]

Received Date
Accepted Date

DOI: 10.1039/xxxxxxxxxx

www.rsc.org/journalname

The interest in organic molecules exhibiting Thermally Activated Delayed Fluorescence (TADF) has been reinvigorated in recent years owing to their potential to be exploited as emitters in highly efficient purely organic light emitting diodes (OLEDs). However, designing new molecules that exhibit efficient TADF is a non-trivial task because they would appear to require the optimisation of a number of contrasting properties. For example these molecules must exhibit rapid conversion between the singlet and triplet manifolds without the use of heavy elements to enhance spin-orbit coupling. They should also display a large fluorescence rate, but simultaneously a small energy gap between low lying singlet and triplet states. Consequently to achieve systematic material design, a detailed understanding of the fundamental factors influencing the photophysical behaviour of TADF emitters is essential. Towards achieving this goal, theory and computation is playing a crucial role. In this feature article the recent progress in the theory of organic TADF molecules in the context of OLEDs is presented, with a view of achieving a deeper understanding of these molecules and driving systematic material design.

1 Introduction

The conventional view of molecular fluorescence is as a two step process. An initial absorption generates an electronically excited state, which subsequently, and ignoring all other possible pathways, decays radiatively into the electronic ground state. This is known as prompt fluorescence. Fluorescence can, depending on competing excited state processes, occur by a more complicated route, the triplet manifold. In this case, the singlet excited state state decays via intersystem crossing (ISC) into the triplet states. Subsequently, if the phosphorescence and non radiative decay of the triplet state is slow and the energy gap between the singlet and triplet states is small enough (normally $\leq$0.2 eV), then a second ISC, often called reverse intersystem crossing (rISC), back to the singlet state occurs followed by emission. This is known as delayed fluorescence (DF) [1].

DF was first reported in solid uranyl salts by Perrin *et al.* [2], and later characterised in more detailed by Lewis *et al.* [3] in rigid media and Parker *et al.* [4] using Eosin. The latter study is responsible for its original name, E-type delayed fluorescence. In 2012 Adachi and co-workers [5], exploited the rISC mechanism of DF, renaming it Thermally Activated Delayed Fluorescence (TADF), to harvest the triplet states of molecules generated under electric excitation within an Organic Light Emitting Diodes (OLEDs) and were able to demonstrate high efficiency electroluminescence for the first time using only organic molecules. This work has been the main driving force for a significant research interest in developing new emitters and understanding the photophysics of the TADF process [6–8].

The huge literature on new TADF emitters illustrates that to date the design of new TADF molecules has largely focused upon large-scale synthetic programs aimed at developing and then exploiting structure-property relationships. However, while these can lead to incremental progress and simple design rules that can be used to manipulate a specific property, such as the emission or absorption wavelength, it is usually unsuccessful in simultaneously controlling all of the required photophysical properties. This is, at least in part, due to the apparent contradictory requirements of TADF emitters. Indeed, to achieve high efficiency these emitters should have a large radiative rate, but also a small gap between the lowest singlet and triplet states. The latter has largely been achieved by charge transfer states, which minimises the exchange energy and therefore the singlet-triplet gap. However this also leads to molecules with small radiative rates. This example emphasises the importance of achieving a full understanding of the photophysical processes involved in TADF in order to move forward with design.

The design of new molecules can also be achieved computationally, and has the potential to significantly speed-up the screening of potential emitters. Gomez *et al.* [9] recently developed a vir-

[a] *Chemistry- School of Natural and Environmental Sciences, Newcastle University, Newcastle upon Tyne, NE1 7RU, United Kingdom. tom.penfold@ncl.ac.uk*
[b] *Physics Department, Durham University, South Road, Durham, DH1 3LE, United Kingdom.*

View Article Online
DOI: 10.1039/C7CC09612G

tual screening method with the capacity to explore the chemical space of 1.6 million molecules. However, at the heart of these approaches are a number of criteria for specific molecular properties and therefore as for experimental design, a detailed understanding of the TADF mechanism must be achieved to optimise these so called descriptors.

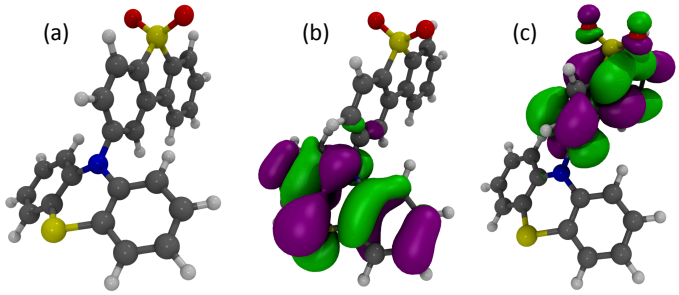

Fig. 1 The structure (a), HOMO (b) and LUMO (c) of 3,7-PTZ-DBTO2.

In this feature article, recent theoretical work aimed at elucidating a full understanding of TADF across a range of time- and lengths scales is discussed. To retain the focus upon the mechanistic aspects of TADF, this article focuses upon a single TADF emitter composed of a phenothiazine donor and a dibenzothiophene-S,S-dioxide acceptor (3,7-PTZ-DBTO2). This structure, highest occupied molecular orbital (HOMO) and lowest unoccupied molecular orbital (LUMO) are shown in Figure 1 [10–12]. While, this is not the highest performing TADF emitter, it represents an excellent prototype to illustrate the key concepts outlined below. For a more detailed discussion about the range of TADF emitters, readers are referred to ref. [6], while for details regarding experimental photophysical characterisation, readers are referred to ref. [8].

2 Kinetics of Thermally Activated Delayed Fluorescence

Initial studies of TADF were interpreted in terms of the equilibrium model, first proposed by Parker *et al.* [4] and later used by Kirchhoff *et al.* [13] to describe the TADF of Cu(I) metal organic complexes. This assumes that $k_F << k_{rISC}$, and therefore the molecule spends sufficient time in the excited state for a equilibrium to form between the singlet and triplet states involved. The relative population of the two states can be expressed using an equilibrium constant:

$$K = \frac{[S_1]}{[T_1]} = \frac{k_{rISC}}{k_{ISC}} = \frac{1}{3}\exp\left\{-\frac{\Delta E_{S_1T_1}}{k_BT}\right\} \quad (1)$$

making it possible to find the rate of the whole TADF process (k_{TADF}), i.e. rISC followed by fluorescence, as the product of the amount of population in the S_1 state and the rate limiting step, i.e. k_F;

$$k_{TADF} = \frac{1}{3}k_F\exp\left\{\frac{-\Delta E_{S_1T_1}}{k_BT}\right\} \quad (2)$$

Importantly, this motivates a design procedure which is based solely upon i) minimising ΔE_{S1-T1} and ii) making the molecule rigid to decrease nonradiative decay. While convenient, the key assumption, i.e $k_{rISC} >> k_F$, must be and often is broken to support new emitters with stronger fluorescence yields [14,15]. In this regime, TADF must be cast in terms of a kinetic process [16], which ignoring non-radiative pathways is written:

$$\frac{dS}{dt} = -(k_F + k_{ISC})[S] + k_{rISC}[T] \quad (3a)$$

$$\frac{dT}{dt} = k_{ISC}[S] - (k_P + k_{rISC})[T] \quad (3b)$$

$$\frac{dG}{dt} = k_F[S] + k_P[T] \quad (3c)$$

G, T and S represent the ground, triplet and singlet states, respectively. k_{ISC} is the rate of ISC, k_{rISC} is the rate of rISC, k_F is the rate of fluorescence, k_P is the rate of phosphorescence. This set of linear differential equations can also be written as:

$$\begin{pmatrix} dS/dt \\ dT/dt \\ dG/dt \end{pmatrix} = \begin{pmatrix} -(k_F+k_{ISC}) & k_{rISC} & 0 \\ k_{ISC} & -(k_P+k_{rISC}) & 0 \\ k_F & k_P & 0 \end{pmatrix} \begin{pmatrix} S(t) \\ T(t) \\ G(t) \end{pmatrix} \quad (4)$$

and integration of these kinetic equations, yielding the time-dependent population of each of the electronic states is obtained using:

$$P(t) = e^{Mt}P(0) \quad (5)$$

where $P(0)$ is the initial (t=0) population of each state and M is the matrix operating on the excited state populations in Equation 4. This equation can now be used to extract the rate of important processes from experimental data.

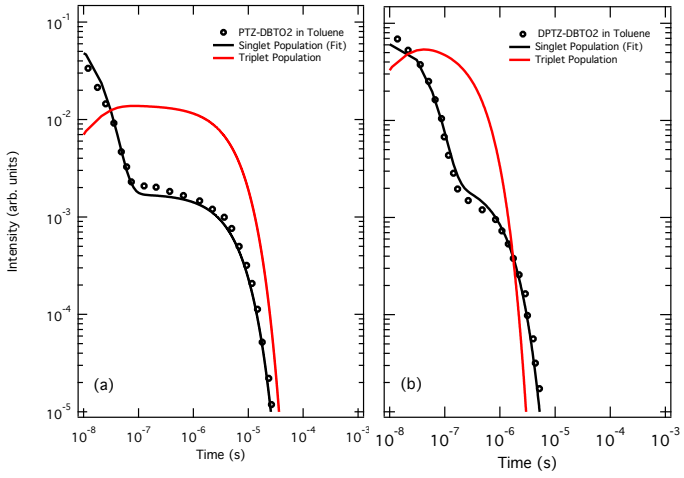

Fig. 2 A fit (black solid line) using Equation 5 of the time-dependent emission intensity (black circles) of 3,7-PTZ-DBTO2 (a) [10,11] and its D-A-D analogue DPTZ-DBTO2 (b) both in toluene. The red line corresponds to the time-dependent population of the triplet states. The fits yields the following parameters k_F=6.0×10^7 s^{-1}, k_{ISC}=1.0×10^7 s^{-1}, k_{rISC}=1.4×10^6 s^{-1} for 3,7-PTZ-DBTO2 and (b) k_f=3.0×10^7 s^{-1}, k_{ISC}=5.0×10^7 s^{-1}, k_{rISC}=4.8×10^6 s^{-1} for DPTZ-DBTO2.

Indeed, Figure 2a shows the experimental emission decay of 3,7-PTZ-DBTO2 in toluene [10] (black circles) plotted with a fit of the time-dependent S_1 population using Equation 5. The best agreement is obtained using k_F= 6×10^7 s^{-1}, k_{ISC}=1×10^7 s^{-1}

View Article Online
DOI: 10.1039/C7CC09612G

and k_{rISC}=1.4×10^6, providing rates determined independently but in good agreement with those reported in ref.[11]. Figure 2b shows the corresponding emission decay for the D-A-D analogue, DPTZ-DBTO2. This complex gives similar photophysics and excellent OLED performance >19 % external quantum efficiency (EQE)[17]. In this case the best fit is achieved using k_F=3.0×10^7 s^{-1}, k_{ISC}=5.0×10^7 s^{-1}, k_{rISC}=4.8×10^6 s^{-1}, also in good agreement with experimental observations[17]. Importantly, the similarity in the photophysics of the two molecules demonstrates that D-A-D-type molecules exhibiting intrinsically more efficient TADF than corresponding D-A molecules[18] cannot be assumed. The advantage of this approach, compared to the usual approach of fitting the prompt and delayed components with exponentials, is that the rates can be extracted. In addition, as shown in Figure 2 (red trace), it naturally provides the time-dependent population of the triplet states. These are important in the context of the roll-off efficiency in OLEDs.

3 The Electronic Structure of TADF Emitters

The first step to understanding the characteristics of a particular TADF emitter is simulating the excited state properties at important geometries on the potential energy surface, such as the ground and excited minima. For larger molecules, for which most TADF emitters can be classed, time-dependent density functional theory (TDDFT)[19,20] is usually the method of choice due to its appealing trade-off between accuracy and computational efficiency. However, the importance of charge-transfer states in the TADF mechanism is at odds with the widely documented limitation of TDDFT for simulating such excitations[21]. Consequently, care must be taken when adopting commonly used functionals, such as PBE0 and B3LYP, as they will underestimate the energy of the CT states. This is most important for emitters involving states of different character, for example a $\pi\pi^*$ and CT state, because the relative energy gap between them will be incorrect. In comparison for the energy gap between the singlet and triplet CT states, although the absolute energy compared to the ground state will be underestimated, their relative energy will be captured. This is helped using TDDFT within the Tamm-Dancoff approximation (TDA)[22], which helps reduce problems associated with the triplet instability[23].

To address these limitations, Huang *et al.*[24], adopted an approach whereby the exchange-correlation functional used was determined using a charge-transfer index defined following an analysis of the HOMO and LUMO orbitals. While the approach has been reasonably widely applied[25–27] and yielded qualitative trends with experimental results, it is not an approach which should be routinely adopted. Indeed, as each *xc* functional does not only vary by the fraction of exact exchange, this approach will not necessarily yield a consistent description of the excited state properties between different systems where different functionals are used.

An alternative approach, proposed by Penfold[28] and later by Sun *et al.*[29] exploited optimally tuned range-separated functionals. In range separated functionals, the amount of exact exchange is weighted according to the inter electron distance, r_{12}:

$$\frac{1}{r_{12}} = \mathrm{erfc}(\mu \cdot r_{12}) \cdot r_{12}^{-1} + \mathrm{erf}(\mu \cdot r_{12}) \cdot r_{12}^{-1} \quad (6)$$

where $\mathrm{erf}(x) = \frac{2}{\sqrt{\pi}} \int_0^x exp(-t^2)dt$ and $\mathrm{erfc}(x) = 1 - \mathrm{erf}(x)$. This provides the flexibility to include more exact exchange at large electron-electron distances, overcoming the limitation of locality for most exchange-correlation functionals in TDDFT. The *optimal tuning* approach was initially proposed by Baer, Kronik, and coworkers who varied μ in order to minimise the energy difference between energy of the HOMO (ε_{HOMO}) and the first ionisation potential (IP) of the neutral system and the energy difference between energy of the HOMO of the anionic system, ε_{HOMO}(N+1) and the electron affinity (EA) of the neutral system.[30]. These conditions are expressed as:

$$J_0(\mu) = |\varepsilon^{\mu}_{HOMO}(N) + IP^{\mu}(N)| \quad (7a)$$

$$J_1(\mu) = |\varepsilon^{\mu}_{HOMO}(N+1) + EA^{\mu}(N)| \quad (7b)$$

Therefore the goal is to minimise the relationship:

$$J(\mu) = J_0(\mu) + J_1(\mu) \quad (8)$$

The results obtained from the simulations in refs[28,29] gave quantitative agreement with experimental observation. Although, it is noted that the optimal value of μ is both molecule and geometry dependent.

Figure 3 shows the experimental absorption spectrum of 3,7-PTZ-DBTO2 in dichloromethane compared to the absorption spectra calculated using the M062X (blue) and optimally tuned LC-BLYP (red) functional. In both cases there is good agreement between the calculated and experimental spectra making it possible to assign each of the features as a mixture of CT and locally excited states on either the donor or acceptor groups. Throughout this work, it has been found that the M062X functional[31] provides a good description of the excited state properties of 3,7-PTZ-DBTO2 and derivatives[10].

The alignment of the important excited states plays a significant role in TADF and is discussed in more detail in section 6, Importantly, this can be dramatically altered by the embedding environment. This is not so apparent from the absorption spectra[15,32], as absorption probes the dielectric response of a material on the optical timescales, i.e. it depends on the polarisability (charactered by squared refractive index) of the environment. Indeed, for environments with higher polarisability the spectrum will be red shifted as observed in ref.[32] for 4CzIPN dissolved in toluene (n^2=2.24), dichloromethane (n^2=2.03), ethanol (n^2=1.85) and acetonitrile (n^2=1.81). Similar trends are also observed for the energy of the S_1 CT state in 3,7-PTZ-DBTO2 in Table 1 (S_1^{qbs}).

For emission the picture is somewhat different. Indeed, because emission probes the longer time dielectric response of the solvent after excitation it is most sensitive to the polarity of the environment. This is especially evident for TADF emitters because of the large difference in the molecular dipole moment between the ground and excited states associated with the CT state. The

View Article Online
DOI: 10.1039/C7CC09612G

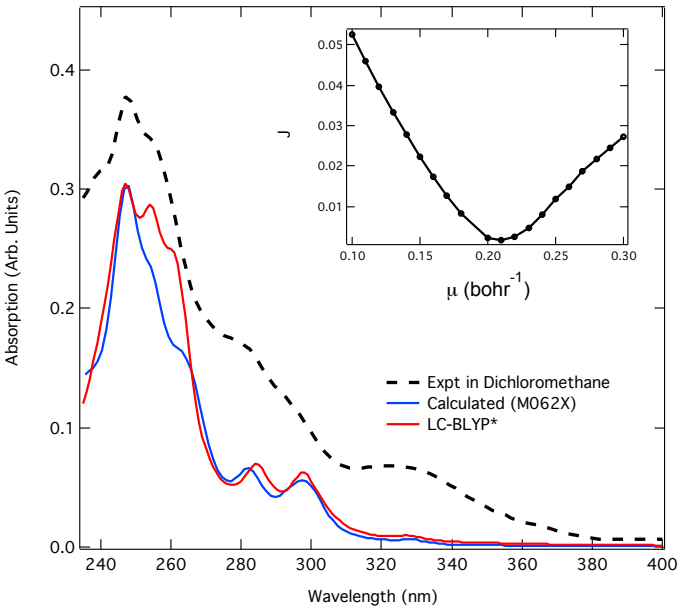

Fig. 3 The experimental absorption spectrum of 3,7-PTZ-DBTO2 in dichloromethane (black dashed line) compared to the absorption spectra calculated using the M062X (blue) and optimally tuned LC-BLYP (red) functional. The inset shows J(μ) used in the tuning of the LC-BLYP functional.

	n^2	ε	S_1^{abs} (eV)	S_1^{em} (eV)	f
in Vacuo	-	-	3.61	2.65	0.0007
in Toluene	2.24	2.37	3.65	1.99	0.0003
in DCM	2.03	8.93	3.69	1.45	0.0002
in Ethanol	1.85	24.85	3.71	1.30	0.0001

Table 1 The energy of the S_1 CT state at the ground (absorption) and S_1 (emission) state geometries of 3,7-PTZ-DBTO2 as a function of solvent polarity (ε). The oscillator strength (f) is calculated at the S_1 (emission) excited state geometry.

emission energy of 3,7-PTZ-DBTO2 is shown in Table 1, and the solvent effect has been incorporated using a state specific polarisable continuum model[33]. In *Vacuo*, the emission occurs at 2.65 eV (467 nm) and corresponds to a Stokes shift derived entirely from the structural changes of 3,7-PTZ-DBTO2 in its excited state of ~1.0 eV. Despite the large Stokes shift, the structural change between the ground and excited state minima is relatively small. The most significant change is an elongation of the C-N bond between the donor and acceptor units, which increases from ~1.43 Å to ~1.48 Å. Importantly, because of the 1/R dependence for the excitation energies of charge-transfer states this small structural change is sufficient to account for the significant Stokes shift. The other change is a nitrogen pyramidisation between the donor and acceptor groups which goes from 130° to 100°, although this has a much smaller effect on the energy of the ^{1}CT state.

Upon inclusion of a state-specific PCM model, which uses the excited state density to calculate the solvent reaction field[33], a distinct solvation effect is observed with the emission energy decreasing significantly with increasing ε as expected. The emission in toluene, ~1.99 eV, is in reasonable agreement with the peak of the emission of 3,7-PTZ-DBTO2 which is approximately ~2.05 eV[11]. Increasing the polarity of the solvent also decreases the oscillator strength because the ^{1}CT is further away from the $\pi\pi^*$ states associated with donor and acceptor groups, decreasing their ability to mix, gaining oscillator strength.

Besides density functional based approaches, Marian has exploited a method based upon a combination of density functional theory/multireference configuration interaction (DFT/MRCI), originally designed by Grimme and Waletzke[34] and later updated by Marian *et al.*[35]. This was applied to study the excited state energetics of 3-(9,9-dimethylacridin-10(9H)-yl)-9H-xanthen-9-one (ACRXTN). Importantly, the presence of multiple states of different character, $n\pi^*$, $\pi\pi^*$ and CT illustrated the limitations of TDDFT, within the approximation of commonly used exchange and correlation functional and emphasised the requirement for great care has to be exercised when TDDFT calculations are employed to aid the experimental assignments.

4 Spin-Vibronic Mechanism for TADF

The crucial component, which is usually rate limiting in determining the lifetime of the triplet states and the TADF process is the rate of rISC (k_{rISC}). Within the Condon approximation, i.e. decoupling electronic and vibrational motion, k_{rISC} between a singlet (ψ_S) and triplet (ψ_T) state can be described using Fermi's golden rule as:

$$k = \frac{2\pi}{3\hbar Z}\sum_f |\langle\psi_T|\hat{\mathscr{H}}_{soc}|\psi_S\rangle|^2 \sum_{k,j} \exp^{-\beta E_k} |\langle\nu_{Tk}|\nu_{Sj}\rangle|^2 \delta(E_S - E_T). \quad (9)$$

where ν are the vibrational energy levels and $\hat{\mathscr{H}}_{so}$ is the spin-orbit Hamiltonian. The δ function ensures the conservation of the molecular energy for the nonradiative transition. Importantly in this case, rISC is driven by direct SOC, i.e. only electronic coupling, which has no dependency upon the vibrational degrees of freedom.

Initial studies assumed that TADF occurred between the ^{1}CT and ^{3}CT states, however theoretical considerations and experimental evidence has clearly demonstrated that this picture is insufficient. Firstly, SOC between two states of the same character is forbidden[36] as any change in spin must be accompanied by a corresponding change in angular momentum, so that total angular momentum is conserved. If the states have the same character, the requirement to have a change in angular momentum cannot be fulfilled. Secondly, Monkman and co-workers[15,37] showed that the states involved in TADF could be independently tuned by the environment and therefore they must be of different character. Subsequently, Ward *et al.*[10] showed that different D-A-D molecules with very similar energy gaps ($\Delta E_{S_1-T_1}$) exhibit large variations in k_{rISC}. They found that by sterically hindering the motion of D and A group, the emission could be switched from TADF to phosphorescence. This indicated a mechanism which is dynamic in nature, in the sense that it depends on molecular vibrations and must therefore go beyond the Condon approximation described in Equation 9.

These observations were explained by Gibson *et al.*[12] who stud-

View Article Online
DOI: 10.1039/C7CC09612G

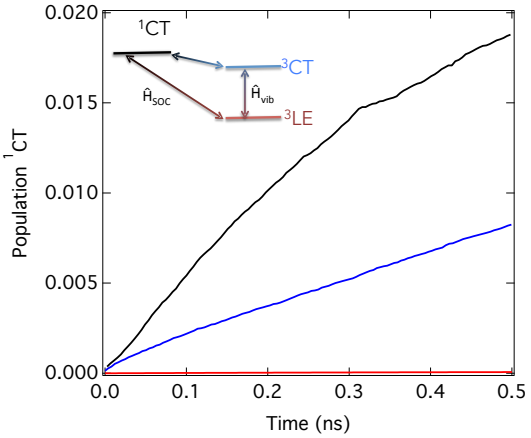

Fig. 4 Population kinetics of the ^{1}CT associated with reverse intersystem crossing after initially populating the ^{3}LE state (see inset). (a) 2,8-PTZ-DBTO2 (black), (b) 3,7-PTZ-DBTO2 (blue) and (c) 2,8-PTZ-DBTO2 without nonadiabatic coupling (red).

ied the rate of rISC in 3,7-PTZ-DBTO2 using quantum dynamics. They found that there were three states, ^{1}CT, ^{3}CT and $^3\pi\pi^*$ important to TADF and used them to set up a model Hamiltonian to describe the mechanism of rISC. Figure 4 shows the population kinetics of the ^{1}CT for 0.5 ns after initial population of the lowest triplet, $^3\pi\pi^*$, state. The blue trace shows the dynamics of 3,7-PTZ-DBTO2, while the red trace shows the same dynamics, but with the nonadiabatic coupling between the $^3\pi\pi^*$ and ^{3}CT states removed. This shows that rISC is quenched in this case and reveals the critical role of vibronic coupling between the two triplet states for the $^3\pi\pi^*$-^{1}CT conversion. Importantly, this cannot be described within first order perturbation theory, Equation 9. These simulations were subsequently supported by experimental observations[38].

Instead TADF must be cast in terms of a spin-vibronic ISC mechanism. In this regime, the molecular excited states cannot be well represented by a simple ladder of states, as depicted in a usual Jablonski diagram. Instead, the interplay amongst spin, electronic and nuclear dynamics leads to mixing and consequently to more complicated spin-vibronic levels. which promote efficient rISC[39]. There are three main mechanisms for spin-vibronic ISC

I Vibrational spin–orbit, e.g. $(\partial\hat{\mathscr{H}}_{SO}/\partial Q_\alpha)Q_\alpha$, in which the size of the SOCME depends on the motion along a particular nuclear degree of freedom, Q_α. This is written to first order, but of course higher-orders can be included if necessary.

II Spin-vibronic, $\hat{\mathscr{T}}_N\hat{\mathscr{H}}_{SO}$, spin–orbit coupling with nonadiabatic coupling between multiple states in the singlet manifold.

III Spin-vibronic, $\hat{\mathscr{H}}_{SO}\hat{\mathscr{T}}_N$, spin–orbit coupling with nonadiabatic coupling between multiple states in the triplet manifold.

Although vibrational spin–orbit is formally different from the interaction terms involving nonadiabatic coupling, in practice these terms can hardly be told apart, and which terms dominate will depend on the system under study. Gibson *et al.*[12] concluded that the third type was most important in 3,7-PTZ-DBTO2. Marian and co-workers recently studied ACRXTN[40] and ACRSA[41] concluding that vibrational spin-orbit was most important. Their work also highlighted that this mechanism is not limited to particular types of states or to only three states. Indeed, in ref.[41] it was found that CT, $\pi\pi^*$ and $n\pi^*$ states were all involved. The Hamiltonian included 6 excited states and found a $k_{rISC} \sim 10^9 s^{-1}$, one of the largest rates reported.

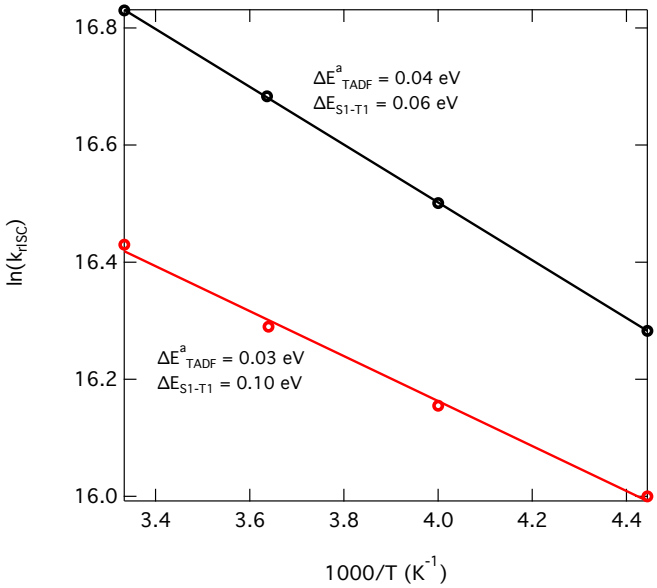

Fig. 5 Energy barrier for TADF, determined from the temperature variation of k_{rISC} plotted against 1000/T (K^{-1}) for two models which have ΔE_{S1-T1} = 0.06 and 0.1 eV. In the case of the latter, the magnitude of nonadiabatic coupling has been doubled to enable these simulations to exhibit sufficient population transfer to S1 at lower temperatures (225 K). Figure reproduced from ref.[42].

The spin-vibronic mechanism provides a unified understanding of the experimental observations for TADF systems. However, it does not lessen the importance of the energy gap between the singlet and triplet states. Experimentally measuring this gap is achieved using two approaches. The first extracts the gap by fitting the integrated DF emission as a function of temperature. It therefore gives a thermal activation energy derived from the Arrhenius equation[8]. The second is the difference between the onset of the fluorescence to phosphorescence signals, i.e. the optical gap. Importantly, it has been repeatedly found that the gap extracted from these two approaches are different, sometimes by a much as 0.35 eV[15]. Indeed, larger differences were generally found for the higher performing molecules. Adachi *et al.*[43] proposed that this difference is due to conformational changes occurring during the rather long transient lifetime of the triplet excited state. Here, coordinate dependent vibronic coupling, alters the adiabatic energy gap between the T_1 and S_1 states. This corresponds to the strong coupling limit in the pioneering paper of Engleman and Jortner[44].

However recently, Gibson *et al.*[42] proposed that the nonadiabatic coupling associated with the spin-vibronic mechanism could also play a significant role in this. Indeed, the nonadiabatic coupling active in the spin-vibronic mechanism, forms an equilibrium between the two lowest triplet states, T_1 ($\pi\pi^*$) and T_2 (^{3}CT), which leads to significant population transfer, even without thermal activation. This lowers the effective activation barrier for TADF because, according to second-order perturbation theory, it becomes dominated by the S_1-T_2 energy gap, rather than the S_1-T_1 energy gap. This is shown in Figure 5 showing the activation energy (ΔE^a) for TADF, determined from the temperature variation of k_{rISC} plotted against 1000/T (K^{-1}) for two models which have ΔE_{S1-T1} = 0.06 and 0.1 eV. In both cases ΔE^a is significantly less than the energy gap. This explanation does not exclude the conclusions of Adachi *et al.*[43], in fact it is expected that to some extent both will be operative. However, as it is desirable to minimise the reorganisation energy in these emitters for high device performance, this nonadiabatic mechanism does offer an alternative design route.

5 Conformational and Regio- Isomerisation

Conformational and Regio- isomerisation are fundamental in chemistry, with profound effects upon physical properties, however their role in excited state properties is less developed. The use of a phenothiazine donor in 3,7-PTZ-DBTO2 means that it can exhibit more than one stable conformer, with both the H-intra and H-extra folded conformers of the phenothiazine possible. This allows formation of parallel quasi-axial (ax) and perpendicular quasi-equatorial (eq) conformers. The nomenclature of axial and equatorial is taken from Stockmann *et al.*[45] and is in reference to the N-S axis and plane of the phenyl rings. The structure, HOMO and LUMO orbitals of the axial form of 3,7-PTZ-DBTO2 is shown in Figure 6, while the *eq* is shown in Figure 1. The main difference is the delocalisation of the HOMO over the whole molecule for the axial form. For the donor-acceptor-donor (D-A-D) molecules there is also the possibility for the mixed conformer, in which one donor is quasi-axial and the other quasi-equatorial.

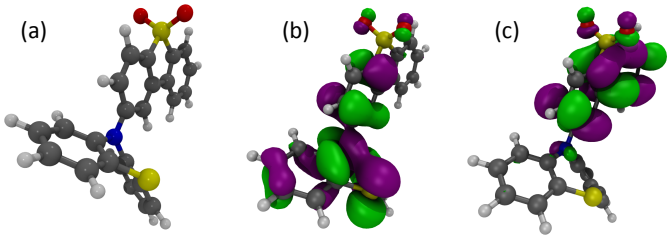

Fig. 6 The structure (a), HOMO (b) and LUMO (c) of quasi-axial conformation of 3,7-PTZ-DBTO2.

Recently, dos Santos *et al.*[46] reported that the conformation of two D-A-D molecules, 2,7- bis(phenothiazin-10-yl)-9,9-dimethylthioxanthene-S,S-dioxide (DPT-TXO2) and 2,7-bis(1-methylphenothiazin-10-yl)-9,9-dimethylthioxanthene-S,S-dioxide (DMePT-TXO2) could be controlled by the polarity of the environment and by the excitation energy. This shows how subtle changes can have a large change on the conformations, but most importantly these conformers exhibit very different TADF performance.

Figure 7a shows the energy of the ground and S_1 energies of the *ax* and *eq* conformers and the transition state between them for 3,7-PTZ-DBTO2 at the optimised ground state geometry (D-A= 1.43 Å). At this geometry the energetics of the axial and equatorial conformers in the ground state are very similar and the most favourable is likely to be strongly influenced by the environment. The dipole moment of the equatorial form is greater, this will be stabilised in polar environments. The barrier between them is >1 eV, meaning that the conformers are essentially locked. In the S_1 state, at the ground state geometry, the equatorial form becomes significantly more stabilised as the localisation of the HOMO and the LUMO orbitals on the donor and acceptors groups respectively makes it a purer CT state. As a consequence it also exhibits a much smaller oscillator strength.

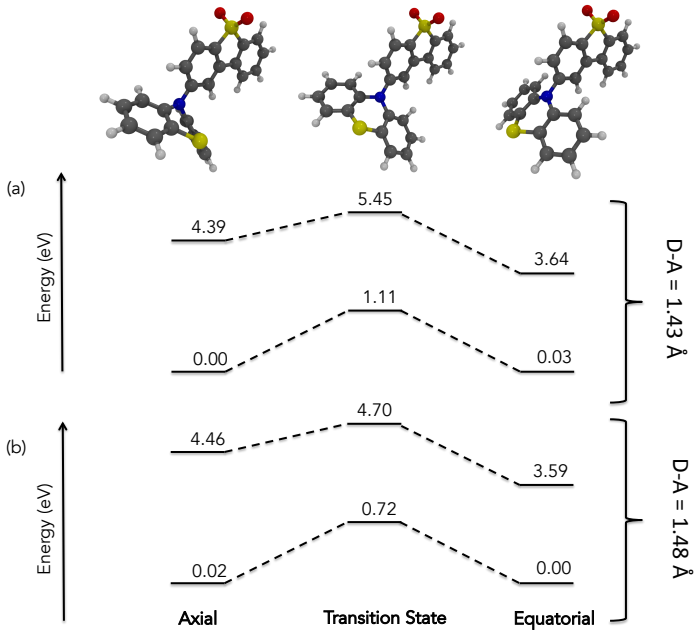

Fig. 7 The energy of the ground and S_1 energies of quasi-axial, quasi-equatorial conformers and the transition state between them for 3,7-PTZ-DBTO2 at the ground state geometry (a) and excited state geometry (b). The latter is generated by elongating the C-N bond between the donor and acceptor groups by 0.05 Å.

The picture is somewhat different in the excited state geometry, where the C-N bond between the donor and acceptor groups is elongated by 0.05 Å. In the ground state of this structure the barrier between the two conformers is lowered by ~0.4 eV, however it remains too high for easy switching between the conformers. In contrast in the excited state the axial form is only 0.24 eV lower than the transition state. This lower barrier means that excess energy, either in the form of heat or excess energy by optical excitation, could switch the axial form into the equatorial conformer. In ref.[47], it was shown that different conformers can have significantly different device performance and therefore considering the potential for multiple conformers, which may or may not have

View Article Online
DOI: 10.1039/C7CC09612G

different TADF performance is important in the context of developing efficient devices.

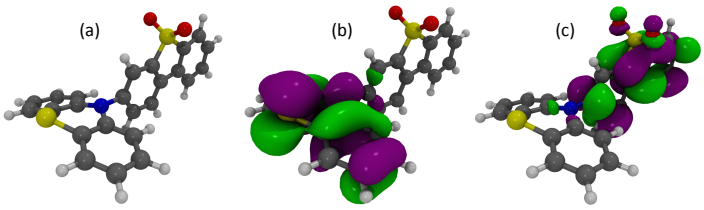

Fig. 8 The structure (a), HOMO (b) and LUMO (c) of 2,8-PTZ-DBTO2.

The effect of regio-isomerisation was recently studied using DPTZ-DBTO2[47] in which the donor group was linked to the 2,8- and 3,7-positions on the acceptor unit. The 2,8-PTZ-DBTO2 regio-isomer is shown in Figure 8, while the 3,7-PTZ-DBTO2 isomer is shown in Figure 1. Although, as shown in Figure 4 (black), the rate of rISC for 2,8-PTZ-DBTO2 is slightly faster than 3,7-PTZ-DBTO2, the oscillator strength of the ^{1}CT state for 2,8-PTZ-DBTO2 is about half that of 3,7-PTZ-DBTO2, reflecting the $\pi^* - n$ and $\pi^* - \pi$ coupling of each to the ground state. This is consistent with a slower prompt fluorescence, but also a significantly slows the delayed fluorescence lifetime and leads a poorer performance in a device[47].

6 The Environment Effect

The strong CT character of the excited state in TADF molecules, places an strong emphasis upon understanding the role of the local environment on TADF emitters.In a device context, the choice of host is especially important as the strong local interactions between the excited state dipole moment of the emitter and the dipole moment of the host can significantly change the emission spectrum. Ishimatsu *et al.*[48] performed one of the first studied into the effect of the environment on the TADF properties using 1,2,3,5- tetrakis(carbazol-9-yl)-4,6-dicyanobenzene (4CzIPN) in four different solvent; toluene, dichloromethane, ethanol, and acetonitrile. They reported that k_{rISC} was significantly enhanced in more polar solvents, due to a smaller ΔE_{ST}. While this reveals the effect of polarity, in this case a solvent molecule is free to reorganise around the excited state dipole moment of the TADF emitter. Crucially, this is not the case in device relevant media, i.e. an amorphous thin film organic solid, where the host is not free to reorient.

While the general principles of Solid State Solvation effects (SSSE) can be seen as analogous to liquid state solvation, the sterically constrained motion of the hosts molecules gives rise to some important differences. Indeed, this can give rise to strong, permanent local electric fields, which will lead to the spectral shifts on the level of individual molecules. But if the fields are random, as one would expect in a completely amorphous solid, then, after averaging over all the molecules in the film, there should be no net shift in either the absorption or emission spectra. Consequently, one might instead expect to observe a spectral broadening, due to the increased dispersion in the absorption and emission energies produced. However, if the molecular orientations are correlated, a net spectral shift could occur[49–51]. Recent simulations have proposed that this alignment between the dipole moment of the guest and the host could be enhanced by emitters which have a sizeable dipole moment already in the ground electronic state[52].

SSSE have been shown to be especially important in 3rd generation OLEDs exploiting TADF[17,37,38,53–58]. The origin of this derives from recent work demonstrating that TADF is not simply a cyclic process between the singlet and triplet CT manifolds, but involves coupling to other states[12,38,40,42,47,59,60], such as local triplet $\pi\pi^*$ (^{3}LE)[12] or $n\pi^*$ states[40]. The effectiveness of the mixing between the states and therefore of the overall TADF process crucially depends energy gap between them. However, while CT states are strongly stabilised in hosts with higher polarity, other states, such as ^{3}LE, will be less so. Crucially this will alter the gap between these states and is likely to significantly change the efficiency of TADF[38].

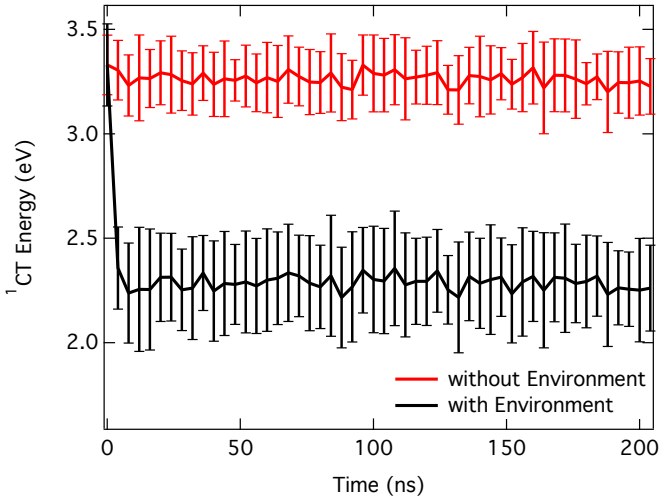

Fig. 9 Time dependence of the S_1 (^{1}CT) state during the first 200 ns after population of the ^{1}CT of 3,7-PTZ-DBTO2 in DPEPO with (black) and without (red) the effect of the local environment. The error bars correspond to the standard deviation of the 20 sampled configurations at each time step.

Besides this static polarity effect, largely analogous to solution phase solvation, a number of interesting subtle effects for TADF emitters in the solid state have also been observed[17,56]. These display a temporal component to their behaviour. After photoexcitation an initial red-shift of the emission is observed. This is associated with the structural rearrangement of the emitter and local embedding environment in the excited state. This red shift continues, albeit at a slower rate into the nanosecond timescale[17,56]. However, from ~100 nanoseconds until the microsecond time frame a pronounced blue-shift is observed. It is noted that the magnitude and the exact timescales of the processes involved are dependent on the particular guest-host combination used.

In recent work, Northey *et al.*[52] used molecular dynamics to study these dynamical SSSE in TADF emitters. Figure 9 shows the time evolution of the ^{1}CT state of 3,7-PTZ-DBTO2 in DPEPO for 200 ns after excitation. A significant stabilisation of the CT state

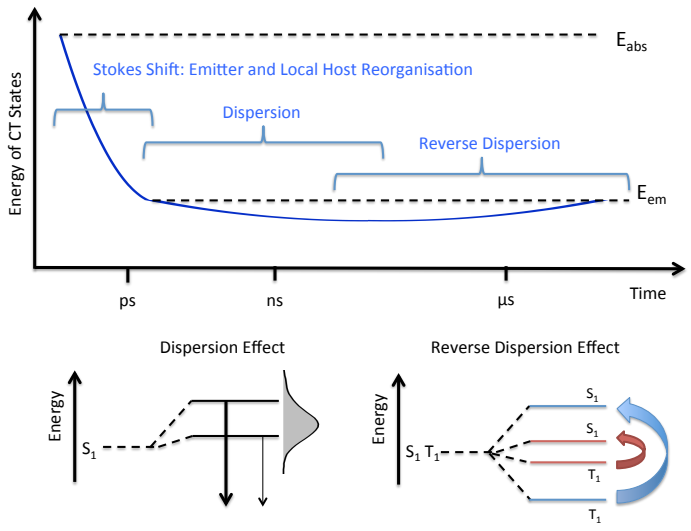

Fig. 10 Schematic of ^{1}CT energetics and the mechanisms responsible, during the excited state lifetime of a TADF emitters in the solid state. The exact timescales do depend on the nature of the guest and host systems involved

is observed within the first 1 ns, which is corresponds to an initial small reorientation of the host molecules. However, subsequently there is no spectral shifts of the emission energy between 20 and 200 ns. This shows that the time dependent red and then blue shift occurring on the nano- and micro- second timescales cannot be a guest-host effect. Instead, it arises from the dispersion of CT conformations present in the solid, whose characteristics are very sensitive to geometric structure. Indeed small changes, for example the dihedral angle between the donor and acceptor groups, can increase the orbital overlap and therefore the exchange energy. This will push the ^{1}CT to higher energy energy, but also increase the oscillator strength meaning it will radiate quicker. Configurations with a purer CT character will emit at lower energies and later in time causing the emission (i.e. before ISC) to red shift. The blue shift observed at longer times can be explained using a similar effect, referred to as reverse dispersion. Those conformations, which have a higher ^{1}CT energy and oscillator strength will also have a larger ΔE_{S-T} and this will slow down the rISC, due to its exponential dependence on the energy gap. Consequently, in contrast to the prompt emission, conformations with the smaller gap will emit first in the delayed component as they are limited by the rISC. This will lead to the later emission exhibiting a blue shift. Overall, this dynamic component will have the effect of broadening the emission spectrum in a device which is undesirable.

7 Conclusions and Perspectives

In this feature article, the recent progress in theoretical and computational chemistry to understand the mechanism of TADF emitters has been discussed. Instead of discussing the plethora of TADF emitters present in the literature, we provided a focused discussion upon a single TADF emitter, namely 3,7-PTZ-DBTO2, to provide insight into the key aspects of the TADF. It is emphasised that the fundamental aspects discussed are generally applicable. These include: i) Efficient TADF operates via a spin-vibronic mechanism, which is dynamic in that it depends on molecular vibrations. ii) Regio- and stereo- isomerisation plays a significant role in the efficiency of the TADF iii) The role of the host molecule is crucial for the performance of TADF, although the behaviour of SSSE cannot be thought of as entirely analogous to solution phase solvation.

One of the the biggest challenges in the application of TADF emitter remains the width of the emission and the outcoupling. For the former, a narrow emission can be achieved by rigidification of the molecule. However, this would work against the spin-vibronic mechanism [12]. Indeed, the roll-off for narrow emitters [61–63] is suggestive of a slower rISC as one would expect given the spin-vibronic mechanism, i.e. making a molecule more rigid will quench the spin-vibronic mechanism. A careful balance must therefore be achieved, and it appears likely that one may need to either choose to sacrifice efficiency for an intrinsically narrow emission or aim for highest performance and mechanically filter unwanted emission

In both cases, a significant enhancement in the EQE could be achieved by increasing the outcoupling, which in the case of randomly orientated emitters places an upper limit of ~30% efficiency on the devices. At present, most TADF system are broadly based upon orthogonally coupled D-A units. However, horizontally alignment within films is best achieved using planar molecules as shown by Kim *et al.* [64]. Recently, Chen *et al.* [65] proposed a new planar molecule, which is coplanar due to intramolecular H-bonding interactions. While the singlet-triplet gap remains too large to efficient TADF, leading to a long delayed fluorescence lifetimes, it represents a promising starting point from which to build. Rajamalli *et al.* [66] have also exploited H-bonding interactions between the donor and acceptor groups to achieve both high outcoupling and narrower emission than standard TADF molecules. In this case, the k_{rISC} appears not to be sacrificed leading to a molecule with a good efficiency even at higher luminance.

An alternative approach to achieve narrow emission and high external quantum efficiencies. developed Adachi and co-workers [67] utilises an efficient fluophore along with TADF materials doped into the host-matrix. In this case, charge recombination occurs at the TADF co-host molecules. However, the co-host is not used for emission, but instead for purely converting the triplet excitons into singlets. It can therefore optimised for maximum rate of reverse intersystem crossing at the sacrifice of the oscillator strength, i.e. its emission lifetime doesn't matter. Emission occurs via singlet energy transfer from the TADF materials (co-host) to the fluophore via Forster resonant energy transfers (FRET). This has been termed hyper-fluorescence technique (also known as TADF-assisted fluorescence). The fluorescence emitter can therefore be chosen with both a large oscillator strength minimising the excited state lifetime and a narrow emission to increase the colour purity. Dexter energy transfer [68] of the triplet states of TADF co-host can be prevented by controlling concentration of the fluophore compared to the concentration of TADF co-host [67] or by using Dendritic Fluorophores [68]. While this is a

View Article Online
DOI: 10.1039/C7CC09612G

promising approach, the energetics makes developing the hyper-fluorescence concept to make efficient blue emitters is extremely challenging. In addition, while this has been studied experimentally, their is presently a need to develop a detailed understanding of the mechanism of hyper-fluorescence, for which theory and computation will play a vital role.

Acknowledgements

The authors thank Prof. Martin Bryce for his contribution to the synthesis of these TADF molecules. TJP acknowledges the EPSRC, Projects EP/N028511/1, EP/R021503/1 and EP/P012388/1 for funding. F. B. D. acknowledges Samsung-SAIT for funding this work using their Global Research Outreach (GRO) Program, and also the EPSRC for funding under grant number EP/L02621X/1. APM acknowledges the EPSRC, Projects EP/L02621X/1 and EP/P012167/1 for funding.

Author biography

Thomas Penfold was awarded his Ph.D. in 2010 from the University of Birmingham, United Kingdom, under the guidance of Prof. Graham Worth. He subsequently joined the group of Prof. Majed Chergui at the École Polytechnique Fédérale de Lausanne, Switzerland before two years within the SwissFEL project at the Paul Scherrer Institut, Switzerland. He joined Newcastle University in 2015 as Lecturer in Theoretical and Computational Chemistry. His current research interests include quantum dynamics, time-resolved spectroscopy and excited state dynamics of organic and inorganic systems.

Fernando B. Dias was awarded his PhD in 2002 from the New University of Lisbon, Portugal, under the supervision of Prof. A. L. Macanita. He then joined Prof. Monkman's group at Durham, UK in 2003, and was appointed as Assistant Professor in Material Physics at Durham University in 2013. Dias has extensive experience on the investigation of the molecular photophysics of organic molecules for application in light emitting diodes and solar cells. Dias' current research is centred on the investigation of the excited state dynamics of molecular emitters, aiming to investigate mechanisms that underpin the observation of thermal activated delayed fluorescence in small molecules and polymers, room temperature phosphorescence in metal-free emitters, and efficient NIR emission in organic emitters.

Andrew P. Monkman was appointed to a Chair in Physics at Durham University in 2002. In 1998 he held a S.T.I.N.T. Visiting Fellowship at the University of Linkoping, Sweden, and was a Leverhulme Fellow in 2002. He has supervised a total of 38 PhD and 13 MSc students. His publications have received >10,500 citations (h-index 53). He has numerous ongoing industrial collaborations for OLEDs, especially for TADF. His research focuses on spectroscopic investigation of luminescent organic materials using optical techniques, combined with electrical and spectroscopic studies of organic electroluminescent devices.

References

1 C. Baleizão and M. N. Berberan-Santos, *J. Chem. Phys.*, 2007, **126**, 204510.
2 R. Delorme and F. Perrin, *J. Phys. Rad. Ser.*, 1929, **10**, 177–186.
3 G. N. Lewis, D. Lipkin and T. T. Magel, *J. Am. Chem. Soc.*, 1941, **63**, 3005–3018.
4 C. Parker and C. Hatchard, *Trans. Faraday Soc.*, 1961, **57**, 1894–1904.
5 H. Uoyama, K. Goushi, K. Shizu, H. Nomura and C. Adachi, *Nature*, 2012, **492**, 234–238.
6 M. Y. Wong and E. Zysman-Colman, *Adv. Mater.*, 2017, **29**,1605444.
7 Z. Yang, Z. Mao, Z. Xie, Y. Zhang, S. Liu, J. Zhao, J. Xu, Z. Chi and M. P. Aldred, *Chem. Soc. Rev.*, 2017, **46**, 915–1016.
8 F. B. Dias, T. J. Penfold and A. P. Monkman, *Methods Appl. Fluoresc.*, 2017, **5**, 012001.
9 R. Gómez-Bombarelli, J. Aguilera-Iparraguirre, T. D. Hirzel, D. Duvenaud, D. Maclaurin, M. A. Blood-Forsythe, H. S. Chae, M. Einzinger, D.-G. Ha, T. Wu *et al.*, *Nat. Mater.*, 2016 , **15**, 1120?1127.
10 J. S. Ward, R. S. Nobuyasu, A. S. Batsanov, P. Data, A. P. Monkman, F. B. Dias and M. R. Bryce, *Chem. Commun.*, 2016, **52**, 2612-2615.
11 R. S. Nobuyasu, Z. Ren, G. C. Griffiths, A. S. Batsanov, P. Data, S. Yan, A. P. Monkman, M. R. Bryce and F. B. Dias, *Advanced Optical Materials*, 2016, **4**, 597-607.
12 J. Gibson, A. Monkman and T. Penfold, *ChemPhysChem*, 2016, **17**, 2956-2961.
13 J. R. Kirchhoff, R. E. Gamache, M. W. Blaskie, A. A. Del Paggio, R. K. Lengel and D. R. McMillin, *Inorg. Chem.*, 1983, **22**, 2380–2384.
14 Q. Zhang, J. Li, K. Shizu, S. Huang, S. Hirata, H. Miyazaki and C. Adachi, *J. Am. Chem. Soc.*, 2012, **134**, 14706–14709.
15 F. B. Dias, K. N. Bourdakos, V. Jankus, K. C. Moss, K. T. Kamtekar, V. Bhalla, J. Santos, M. R. Bryce and A. P. Monkman, *Adv. Mater.*, 2013, **25**, 3707–3714.
16 F. B. Dias, *Philos. Trans. Royal Soc. A*, 2015, **373**, 20140447.
17 F. Dias, J. Santos, D. Graves, P. Data, R. Nobuyasu, M. Fox, A. Batsanov, T. Palmeira, M. Berberan-Santos, M. Bryce and A. Monkman, *Adv. Sci.*, 2016, **3**, 1600080.
18 X.-K. Chen, S.-F. Zhang, J.-X. Fan and A.-M. Ren, *J. Phys. Chem. C*, 2015, **119**, 9728-9733.
19 A. Dreuw and M. Head-Gordon, *Chem. Rev.*, 2005, **105**, 4009–4037.
20 C. Ullrich, *Time-Dependent Density-Functional Theory*, Oxford Graduate Texts, 2011.
21 A. Dreuw, J. Weisman and M. Head-Gordon, *J. Chem. Phys.*, 2003, **119**, 2943–2946.
22 S. Hirata and M. Head-Gordon, *Chem. Phys. Lett.*, 1999, **314**, 291–299.
23 M. J. Peach, M. J. Williamson and D. J. Tozer, *J. Chem. Theory Comput.*, 2011, **7**, 3578–3585.

View Article Online
DOI: 10.1039/C7CC09612G

24 S. Huang, Q. Zhang, Y. Shiota, T. Nakagawa, K. Kuwabara, K. Yoshizawa and C. Adachi, *J. Chem. Theory Comput.*, 2013, **9**, 3872–3877.

25 S. Wu, M. Aonuma, Q. Zhang, S. Huang, T. Nakagawa, K. Kuwabara and C. Adachi, *J. Mater. Chem. C*, 2013, **2**, 421.

26 Q. Zhang, H. Kuwabara, W. J. Potscavage, Jr., S. Huang, Y. Hatae, T. Shibata and C. Adachi, *J. Am. Chem. Soc.*, 2014, **136**, 18070-18081.

27 Q. Zhang, B. Li, S. Huang, H. Nomura, H. Tanaka and C. Adachi, *Nature Photonics*, 2014, **8**, 326–332.

28 T. J. Penfold, *J. Phys. Chem. C*, 2015, **119**, 13535-13544.

29 H. Sun, C. Zhong and J.-L. Bredas, *J. Chem. Theory Comput.*, 2015, **11**, 3851–3858.

30 R. Baer, E. Livshits and U. Salzner, *Ann. Rev. Phys. Chem.*, 2010, **61**, 85–109.

31 Y. Zhao and D. G. Truhlar, *Theor. Chem. Acc*, 2007, **120**, 215–241.

32 R. Ishimatsu, S. Matsunami, K. Shizu, C. Adachi, K. Nakano and T. Imato, *J. Phys. Chem. A*, 2013, **117**, 5607–5612.

33 R. Improta, V. Barone, G. Scalmani and M. J. Frisch, *J. Chem. Phys.*, 2006, **125**, 054103.

34 S. Grimme and M. Waletzke, *J. Chem. Phys.*, 1999, **111**, 5645–5655.

35 I. Lyskov, M. Kleinschmidt and C. M. Marian, *J. Chem. Phys.*, 2016, **144**, 034104.

36 C. M. Marian, *Wiley Interdiscip Rev Comput Mol Sci.*, 2011, **2**, 187–203.

37 P. L. Santos, J. S. Ward, P. Data, A. S. Batsanov, M. R. Bryce, F. B. Dias and A. P. Monkman, *J. Mater. Chem. C*, 2016.

38 M. K. Etherington, J. Gibson, H. F. Higginbotham, T. J. Penfold and A. P. Monkman, *Nat. Comm.*, 2016, **7**, 13680.

39 T. J. Penfold, E. Gindensperger, C. Daniel and C. Marian, *Chemical Reviews*, DOI: 10.1021/acs.chemrev.7b00617 2017.

40 C. M. Marian, *J. Phys. Chem. C*, 2016, **120**, 3715-3721.

41 I. Lyskov and C. M. Marian, *The Journal of Physical Chemistry C*, 2017, **121**, 21145-21153.

42 J. Gibson and T. Penfold, *Phys. Chem. Chem. Phys.*, 2017, **19**, 8428–8434.

43 S. Hirata, Y. Sakai, K. Masui, H. Tanaka, S. Y. Lee, H. Nomura, N. Nakamura, M. Yasumatsu, H. Nakanotani, Q. Zhang, K. Shizu, H. Miyazaki and C. Adachi, *Nat. Mater.*, 2015, **14**, 330-6.

44 R. Englman and J. Jortner, *Mol. Phys.*, 1970, **18**, 145–164.

45 A. Stockmann, J. Kurzawa, N. Fritz, N. Acar, S. Schneider, J. Daub, R. Engl and T. Clark, *J. Phys. Chem. A*, 2002, **106**, 7958–7970.

46 P. L. dos Santos, J. S. Ward, A. S. Batsanov, M. R. Bryce and A. P. Monkman, *J. Phys. Chem. C*, 2017, **121**, 16462–16469.

47 M. K. Etherington, F. Franchello, J. Gibson, T. Northey, J. Santos, J. S. Ward, H. F. Higginbotham, P. Data, A. Kurowska, P. L. Dos Santos *et al.*, *Nat. Comm.*, 2017, **8**, 14987.

48 R. Ishimatsu, S. Matsunami, K. Shizu, C. Adachi, K. Nakano and T. Imato, *J. Phys. Chem. A*, 2013, **117**, 5607–5612.

49 V. Bulović, A. Shoustikov, M. Baldo, E. Bose, V. Kozlov, M. Thompson and S. Forrest, *Chem. Phys. Lett.*, 1998, **287**, 455–460.

50 V. Bulović, R. Deshpande, M. Thompson and S. Forrest, *Chem. Phys. Lett.*, 1999, **308**, 317–322.

51 M. Baldo, Z. Soos and S. Forrest, *Chem. Phys. Lett.*, 2001, **347**, 297–303.

52 T. Northey, J. Stacey and T. Penfold, *J. Mater. Chem. C*, 2017, **5**, 11001–11009.

53 J. Lee, K. Shizu, H. Tanaka, H. Nomura, T. Yasuda and C. Adachi, *J. Mater. Chem. C*, 2013, **1**, 4599.

54 R. Noriega, E. S. Barnard, B. Ursprung, B. L. Cotts, S. B. Penwell, P. J. Schuck and N. S. Ginsberg, *J. Am. Chem. Soc.*, 2016, **138**, 13551–13560.

55 P. L. dos Santos, J. S. Ward, M. R. Bryce and A. P. Monkman, *J. Phys. Chem. Lett.*, 2016, **7**, 3341–3346.

56 G. Méhes, K. Goushi, W. J. Potscavage and C. Adachi, *Org. Elec.*, 2014, **15**, 2027–2037.

57 J. Fan, L. Lin, and C-K. Wang, *J. Mater. Chem. C*, 2017, **5**, 8390–8399.

58 J. Fan, L. Lin, and C-K. Wang, *Org. Elec.*, 2017, **51**, 349–356.

59 R. Huang, J. Avó, T. Northey, E. Chaning-Pearce, P. L. dos Santos, J. S. Ward, P. Data, M. Etherington, M. A. Fox, T. J. Penfold *et al.*, *J. Mater. Chem. C*, 2017, **5**, 11001-11009.

60 T. Kobayashi, A. Niwa, K. Takaki, S. Haseyama, T. Nagase, K. Goushi, C. Adachi and H. Naito, *Phys. Rev. Appl.*, 2017, **7**, 034002.

61 Y. J. Cho, S. K. Jeon, S.-S. Lee, E. Yu and J. Y. Lee, *Chem. Mater.*, 2016, **28**, 5400–5405.

62 T. Hatakeyama, K. Shiren, K. Nakajima, S. Nomura, S. Nakatsuka, K. Kinoshita, J. Ni, Y. Ono and T. Ikuta, *Adv. Mater.*, 2016, **28**, 2777–2781.

63 L. Lin, J. Fan, L. Cai, and C-K Wang, *Mol. Phys.*, 2018, **116**, 19–28.

64 D. Kim, K. Inada, L. Zhao, T. Komino, N. Matsumoto, J. Ribierre and C. Adachi, *J. Mater. Chem. C*, 2017, **5**, 1216–1223.

65 X.-K. Chen, Y. Tsuchiya, Y. Ishikawa, C. Zhong, C. Adachi and J.-L. Brédas, *Adv. Mater.*, 2017, **29**, 1702767.

66 P. Rajamalli, N. Senthilkumar, P.-Y. Huang, C.-C. Ren-Wu, H.-W. Lin and C.-H. Cheng, *J. Am. Chem. Soc.*, 2017, **139**, 10948–10951.

67 H. Nakanotani, T. Higuchi, T. Furukawa, K. Masui, K. Morimoto, M. Numata, H. Tanaka, Y. Sagara, T. Yasuda and C. Adachi, *Nat. Comm.*, 2014, **5**, 4016.

68 N. Aizawa, S. Shikita and T. Yasuda, *Chem. Mater.*, 2017, **29**, 7014–7022.